In memory of Professor Robert R. Gałązka

Topological Phase Diagram of Semimagnetic Semiconductor $Pb_{1-x-y}Sn_xMn_yTe$

A. Łusakowski[a,*], P. Bogusławski[a] and T. Story[a,b]

[a] *Institute of Physics, Polish Academy of Sciences, al. Lotników 32/46, PL-02668 Warsaw, Poland*
[b] *International Research Centre MagTop, Institute of Physics, Polish Academy of Sciences, al. Lotników 32/46, PL-02668 Warsaw, Poland*

Doi: 10.12693/APhysPolA.141.156 *e-mail: lusak@ifpan.edu.pl

Local density approximation is used to study the band structure of $Pb_{1-x}Mn_xTe$ and $Pb_{1-x-y}Sn_xMn_yTe$ alloys with about 6% of cation sites occupied by magnetic Mn ions. The topological phase diagram as a function of chemical composition, hydrostatic pressure, and magnetization is presented. Three phases: normal, topological crystalline insulator, and Weyl semimetal are identified. The possibility of transitions between these phases induced by the external magnetic field and crystal deformation is analysed.

topics: semimagnetic semiconductors, topological insulators

1. Introduction

The IV–VI mixed crystals $Pb_{1-x}Sn_xTe$, $Pb_{1-x}Sn_xSe$ and $Pb_{1-x-y}Sn_xMn_yTe$ are narrow gap semiconductors crystallizing in the rock salt structure [1, 2]. By changing the chemical composition, external pressure, or temperature, it is possible to drive a transition from the trivial insulator to the topological crystalline insulator (TCI) phase. In the mentioned alloys, the mirror symmetry with respect to the (110) crystallographic planes [3–6] is responsible for the presence of a nontrivial topological phase in the bulk, and of the zero-gap Dirac-like states on certain high-symmetry crystal facets. Recently, we analysed the influence of Mn ions on the topological properties of $Pb_{1-x-y}Sn_xMn_yTe$ [7]. In particular, we predicted that an external magnetic field or the presence of low-temperature spontaneous magnetization in $Pb_{1-x-y}Sn_xMn_yTe$ can induce a transition from the trivial as well as from the nontrivial phase to the Weyl semimetal (WSM) phase.

Let us remind that WSM is a system in which the conduction and valence bands touch each other at an even number of isolated points in the momentum space in the first Brillouin zone — the system's energy gap is therefore zero. Each of these points, also known as the Weyl node, has an interesting topological property, namely, the calculation of the Berry flux through the surface surrounding a single node gives an integer number called topological charge equal to ± 1. Since the total topological charge in the first Brillouin zone is always zero in semimetals, the number of the Weyl nodes must be even. In contrast to the Dirac semimetals, in Weyl systems the linearly dispersing electronic states of a given cone are nondegenerate.

We recently performed calculations of the band structure and topological properties for $Pb_{1-x}Sn_xTe$ [8] and $Pb_{1-x-y}Sn_xMn_yTe$ [7]. Our analysis shows that the zero energy gap regions between the topologically trivial and nontrivial phases are of a nonzero width as a function of a lattice parameter or tin concentration. Let us stress that these zero energy gap regions are mainly due to the presence of different cations in the system, i.e, the different chemical properties of lead and tin. Later, Wang et al. [9] have noticed that these zero energy gap regions may be considered the WSM phases. The experimental confirmation of the existence of this region is very difficult, because in IV–VI semiconductors it is very problematic to grow a crystal with a vanishing free carrier concentration. In the literature on the subject, we found only one work that may confirm our predictions [10].

In this short communication, we analyse the influence of magnetization due to the manganese ions on the range of existence of the WSM phase and present two experimentally relevant topological phase diagrams. In the first one, the control parameters are magnetization and the lattice parameter for $Pb_{1-x}Mn_xTe$ ($x \approx 6\%$), while in the second case we consider the variations of magnetization and the Sn concentration for $Pb_{1-x-y}Sn_xMn_yTe$ ($y \approx 6\%$).

2. Technical details of calculations

Ab initio calculations are done using the OpenMX package [11]. We use local density approximations with the Ceperly–Alder [12] exchange-correlation functional. Pseudopotentials for Pb and Te were generated previously [13], and those for Sn and Mn were taken from the package.

We employ $2 \times 2 \times 2$ supercells containing 64 atoms, 32 cations and 32 tellurium atoms. In the case of $Pb_{1-x}Mn_xTe$, two Pb atoms are replaced by two Mn atoms, corresponding to the composition of 6.25 at.%. In this case, we consider crystals possessing two symmetries: cubic and tetragonal. The latter holds when the crystal is grown epitaxially on a substrate that is not fully lattice matched. In all the cases, the Mn ions are placed in the middle and at the corner of supercells. Due to the difference in ionic radius between Mn and Pb, the Mn–Te and Pb–Te nearest neighbour distances differ as well. To estimate the effect of those microscopic lattice distortions on the band structure for cubic crystals, we compare two cases: that of the ideal lattice and that with fully relaxed Mn–Te and Pb–Te bonds. In the first case, all the atoms are at ideal rock salt lattice sites, and in the second case, the positions of Te atoms surrounding Mn atoms are relaxed. The experimental distance between Pb and Te in this alloy is approximately 3.23 Å, while the distance between Mn and Te is only 2.95 Å. We use these values without any further optimization of the alloy geometry. For $Pb_{1-x-y}Sn_xMn_yTe$, the cations distribution in supercells are chosen according to the special quasirandom structures method [14], and the atomic positions are relaxed to find the ground state configuration like in [7].

The important feature of the OpenMX package is the ability to fix spin directions of atoms in the supercell, in this case, the directions of the Mn spins. The method is based on the material presented in technical notes [15] and was also briefly described in [16]. It allows us to gradually change the relative orientation of spins of the two Mn ions in the supercell from ferromagnetic (FM) oriented along the [001] direction, to antiferromagnetic (AFM), by changing the angle between the Mn spins. There are no constrains imposed on the remaining atoms. After optimizing atomic configurations, we find the final magnetization due to Mn ions. This procedure is supposed to model different degrees of Mn spin polarization, from the maximal one to the paramagnetic case with vanishing Mn magnetization. We aim to avoid costly calculations employing large supercells and averages over several Mn configurations.

The OpenMX package also provides tight binding parameters, which enables efficient calculations of energy bands on a dense k-point mesh in the Brillouin zone. This way, we can determine the number of Weyl points for a given magnetization and chemical composition of $Pb_{1-x-y}Sn_xMn_yTe$. The nonzero number of the Weyl nodes implies that the system is in the Weyl semimetal phase. The same procedure can be applied to $Pb_{1-x}Mn_xTe$. However, in this case, a more efficient method is to fix the angle between the two Mn spins in the supercell and calculate the dependence of the absolute value of the energy gap $E_{\rm gap}$ on the lattice parameter.

3. Results

The calculated dependence of the absolute value of the band gap on the lattice parameter is shown in Fig. 1 for tetragonal $Pb_{0.94}Mn_{0.06}Te$. In the considered case, a biaxial compression in the (001) plane is assumed, and the perpendicular lattice parameter $a_\perp$ is determined by the in-plane $a_\parallel$ lattice parameter in accordance with the assumed Poisson ratio $\nu = -0.3$ for the equilibrium lattice parameter of 6.46 Å.

Three relative orientations of the two Mn ions in the supercell are considered. Angles 0° and 180° correspond to the FM and the AFM spin orientations, respectively, and the results for the intermediate case of 80° are also shown. With decreasing $a_\parallel$, $E_{\rm gap}$ decreases as well and changes its value to negative. The transition from positive to negative band gap occurs in the finite window of pressures (lattice parameters), even when the magnetization vanishes. This effect stems from the broadening of levels originating in the alloy disorder (see [8]) which is neglected in Fig. 2 (see the discussion in Sect. 4).

As it follows from Fig. 1, on both sides of the zero energy gap regions the dependences $E_{\rm gap}$ versus lattice parameter are nearly linear, and thus it is possible to accurately determine the region in which the band gap vanishes.

Before reporting the results of the *ab initio* calculations, let us outline qualitatively what is the expected influence of manganese spin polarization on the phase diagrams — magnetization versus lattice

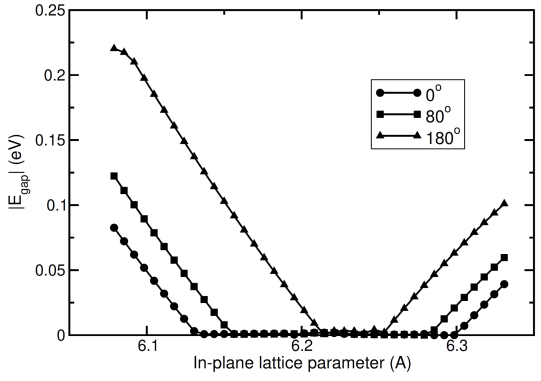

Fig. 1. Dependencies of the modulus of energy gap on the in-plane (001) lattice parameter for three chosen angles between Mn spins for tetragonally distorted crystals $Pb_{1-x}Mn_xTe$. The distorsion is described by the Poisson ratio $\nu = -0.3$ with equilibrium lattice parameter equal to 6.46 Å.

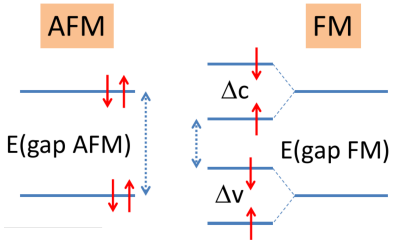

Fig. 2. Schematic view of the conduction and valence band *sp–d* exchange splittings caused by a nonzero Mn spin polarization.

parameter for $Pb_{1-x}Mn_xTe$ or magnetization versus tin concentration for $Pb_{1-x-y}Sn_xMn_yTe$. For simplicity, in this qualitative analysis we concentrate on the $Pb_{1-x}Mn_xTe$ system. For zero spin polarization, the decrease of the lattice parameter leads to the decrease of the energy gap down to zero when the system attains the WSM phase. Further decrease of the lattice parameter drives the system into a nontrivial topology state, the energy gap opens again and (being negative) increases its modulus. It is well known that the spin polarized magnetic ions lead to the spin splitting of both the conduction and the valence bands controlled by *sp–d* exchange coupling [17, 18]. This is shown in Fig. 2, which schematically explains the main factors determining the topological phase diagram of $Pb_{1-x}Mn_xTe$. Figure 2 shows the conduction band minimum (CBM) and the valence band maximum (VBM) together with spins of carriers. Importantly, the result highlights the difference between $E_{\rm gap}$ in the case of the AFM and the FM configurations of the Mn ions. By the case of AFM, we understand the situation of the vanishing spin polarization of the Mn ions as the spin splittings of the bands vanish. In this case, there is no spin splitting, the bands are double degenerate. Consequently, the band gap $E_{\rm gap}$(AFM) is higher than in the case of FM, where $E_{\rm gap}$(FM) is reduced by

$$\Delta E_{\rm gap} = E_{\rm gap}({\rm AFM}) - {\rm E}_{\rm gap}({\rm FM}) = \frac{1}{2}(\Delta_{\rm c} + \Delta_{\rm v}), \quad (1)$$

where Δ_c (Δ_v) is the spin splitting of the CBM (VBM). These spin splittings cause the decrease of the energy gap, which results in earlier attainment of the WSM phase when the lattice parameter decreases. Due to the same reason, the transition between WSM and TCI phases takes place for smaller lattice parameters for nonzero Mn spin polarization. This is shown in Fig. 1.

Figure 3 presents the phase diagram for $Pb_{1-x}Mn_xTe$. One can see that the increasing pressure, i.e, the decreasing lattice parameter, drives the transition from the normal (N) to the WSM phase and then to the TCI phase with a negative band gap. The corresponding range of the lattice parameter widens with increasing magnetization.

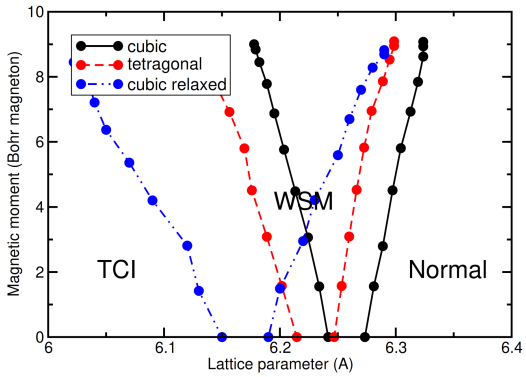

Fig. 3. Calculated topological phase diagram for $Pb_{1-x}Mn_xTe$ with $x \approx 0.06$, which corresponds to a 64-atom supercell with 2 Mn ions. The two parameters are the lattice parameter controlled by hydrostatic pressure (solid line) or layer compression in [001] plane (broken line) and the mean magnetic moment. For comparison we show also topological phase diagram for cubic relaxed system. The values of magnetic moment are given for 2 Mn ions.

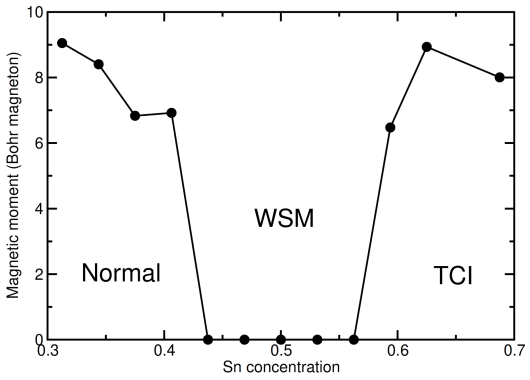

Fig. 4. Calculated topological phase diagram for $Pb_{1-x-y}Sn_xMn_yTe$ with $y \approx 0.06$, which corresponds to a 64-atom supercell with 2 Mn ions. The two parameters are the Sn concentration and the mean magnetic moment. The values of magnetic moment are given for 2 Mn ions.

For small lattice parameters the band gap is negative (inverted), whereas it is positive for larger lattice parameters which corresponds to a topologically trivial situation).

For $Pb_{1-x-y}Sn_xMn_yTe$ crystals, the transition between the normal and the TCI phases is mainly driven by the increase of Sn content rather than the changes of lattice parameters. However, the main ideas of the above analysis apply also to this case.

In Fig. 4 we present the phase diagram for $Pb_{1-x-y}Sn_xMn_yTe$ for a varying Sn concentration. We recall that in the case of $Pb_{1-x}Sn_xTe$, the increase in the Sn content drives the N-to-TCI transition, and the intermediate WSM phase is related to the alloy broadening of the energy bands [7]. From Fig. 3 it follows that the presence of Mn makes the

Sn content window of the WSM phase wider, even in the absence of magnetization. Increasing magnetization considerably widens this window.

One can observe that the boundary between the normal and the WSM phase is not monotonic. We ascribe this effect to the limited accuracy of the special quasirandom structures method. Averaging over many atomic configurations with fixed x and y would make the boundary smooth. We met similar problems in our previous papers [7, 8].

4. Discussion

Changes in the lattice parameter of a given sample can be realized either by changing temperature or by applying external pressure. Both methods were previously experimentally examined. The thermal expansion coefficient for IV–VI semiconductors is of the order of 2×10^{-5} K^{-1}, thus the decrease of the temperature by 200 K reduces a by 0.025 Å. Alternatively, hydrostatic pressure of 5 GPa decreases the PbTe lattice parameter from $a_0 = 6.46$ Å(at $T = 300$ K) to 6.26 Å [19]. In these cases, the crystal retains its cubic symmetry.

On the other hand, the crystalline structure of layered epitaxial heterostructures is typically characterized by a biaxial crystal deformation brought about by lattice mismatch or by thermal expansion mismatch between a $Pb_{1-x-y}Sn_xMn_yTe$ layer and the substrate or a buffer layer. In such situations, the symmetry is lowered to tetragonal. In particular, in $Pb_{1-x}Mn_xTe$ and $Pb_{1-x-y}Sn_xMn_yTe$ epitaxially grown on BaF_2 or KCl, the in-plane lattice deformations $\delta a/a$ are of the order of 0.1% or −0.5%, respectively [2, 20].

Given the above possibilities, the predicted phase diagrams for $Pb_{1-x}Mn_xTe$ shown in Fig. 3 can be verified experimentally by the application of hydrostatic pressure. The changes of temperature or the lattice mismatch effects appear too small to drive a system in interesting regions of the diagram.

The $Pb_{1-x-y}Sn_xMn_yTe$ case shown in Fig. 3 can be verified experimentally. We are aware, however, that in this case the main experimental difficulty is caused by high hole concentrations originating from high concentrations of Sn vacancies. For this reason, it will be very difficult to obtain crystals in which the WSM phase can be studied. But, as it was shown in [10], for $Pb_{1-x}Sn_xTe$ it is possible.

In both Figs. 3 and 4, the averaged z-component of the magnetic moment is considered as a free parameter. Its magnitude is determined by the external magnetic field and temperature. We also note that $Pb_{1-x-y}Sn_xMn_yTe$ at sufficiently high Mn concentration and sufficiently low temperatures spontaneously transforms to the FM phase, while magnetization vanishes at vanishing magnetic field and sufficiently high temperatures [21, 22]. The window in which the WSM phase is stable depends on the magnetization M, and it increases with the increasing M.

As it was mentioned, the considered ranges of parameters are realistic from the experimental point of view. Thus, it seems that the phase diagrams shown in Figs. 3 and 4 can be verified experimentally.

5. Conclusions

Theoretical topological phase diagram of $Pb_{1-x}Mn_xTe$ and $Pb_{1-x-y}Sn_xMn_yTe$ containing $\approx$ 6 at.% of Mn was calculated. We find that, depending on the chemical composition, hydrostatic pressure, and magnetization (the latter being determined by the composition, external magnetic field, and temperature), those alloys assume the normal phase, the Weyl semimetal phase, or the topological crystal insulator phase. The possibility of transitions between them induced by the magnetization is addressed in detail. We also consider an experimentally relevant case of tetrahedrally deformed epitaxial layers of $Pb_{1-x}Mn_xTe$. In practice, the Mn spin polarization can be controlled by an external magnetic field, which implies that the band gap can be tuned. That opens the possibility of the controlled transitions between the N, WSM and TCI phases.

Acknowledgments

This work was partially supported by the National Science Centre NCN (Poland) projects UMO-2016/23/B/ST3/03725 (AŁ), UMO-2017/27/B/ST3/02470 (AŁ) as well as by the Foundation for Polish Science through the IRA Programme co-financed by EU within SG OP (TS).

References

[1] G. Nimtz, B. Schlicht, in: *Narrow-Gap Semiconductors*, Ed. G. Höhler, *Springer Tracts in Modern Physics*, Vol. 98, Springer-Verlag, Berlin 1983.

[2] *Lead Chalcodenides: Physics and Applications*, Ed. D.R. Khoklov, Taylor and Francis, New York 2003.

[3] T.H. Hsieh, H. Lin, J. Liu, W. Duan, A. Bansil, L. Fu, *Nat. Comm.* **3**, 982 (2012).

[4] P. Dziawa, B.J. Kowalski, K. Dybko, R. Buczko, A. Szczerbakow, M. Szot, E. Łusakowska, T. Balasubramanian, B.M. Wojek, M.H. Berntsen, O. Tjernberg, T. Story, *Nat. Mater.* **11**, 1023 (2012).

[5] Y. Tanaka, Z. Ren, T. Sato, K. Nakayama, S. Souma, T. Takahashi, K. Segawa, Y. Ando, *Nat. Phys.* **8**, 800 (2012).

[6] S.-Y. Xu, C. Liu, N. Alidoust et al., *Nat. Commun.* **3**, 1192 (2012).

[7] A. Łusakowski, P. Bogusławski, T. Story, *Phys. Rev. B* **103**, 045202 (2021).

[8] A. Łusakowski, P. Bogusławski, T. Story, *Phys. Rev. B* **98**, 125203 (2018).

[9] Z. Wang, Q. Liu, J.-W. Luoc, A. Zunger, *Mater. Horiz.* **6**, 2124 (2019).

[10] T. Liang, S. Kushwaha, J. Kim, Q. Gibson, J. Lin, N. Kioussis, R.J. Cava, N.P. Ong, *Sci. Adv.* **3**, e1602510 (2017).

[11] OpenMX, www.openmx-square.org.

[12] D.M. Ceperley, B.J. Alder, *Phys. Rev. Lett.* **45**, 566 (1980).

[13] A. Łusakowski, P. Bogusławski, T. Radzyński, *Phys. Rev. B* **83**, 115206 (2011).

[14] A. Zunger, S.-H. Wei, L.G. Ferreira, J.E. Bernard, *Phys. Rev. Lett.* **65**, 353 (1990).

[15] Taisuke Ozaki, OpenMX, Technical notes, Constrained Non-Collinear Density Functional Theory Implemented in OpenMX.

[16] A. Lusakowski, P. Bogusławski, T. Story, *J. Phys.Condens. Matter* **27**, 226002 (2015).

[17] J.A. Gaj, J. Ginter, R.R. Gałązka, *Phys. Status Solidi* **B89**, 655 (1978).

[18] J.K. Furdyna, *J. Appl. Phys.* **64**, R29 (1988).

[19] R. Minikayev, F. Safari, A. Katrusiak, W. Szuszkiewicz, A. Szczerbakow, A. Bell, E. Dynowska, W. Paszkowicz, *Crystals* **11**, 1063 (2021).

[20] A. Stachow-Wójcik, T. Story, W. Dobrowolski, M. Arciszewska, R.R. Gałązka, M.W. Kreijveld, C.H.W. Swüste, H.J.M. Swagten, W.J.M. de Jonge, A. Twardowski, A.Yu. Sipatov, *Phys. Rev. B* **60**, 15220 (1999).

[21] P. Lazarczyk, T. Story, M. Arciszewska, R.R. Galazka, *J. Magn. Magn. Mater.* **169**, 151 (1997).

[22] G.P. Mazur, K. Dybko, A. Szczerbakow, J.Z. Domagala, A. Kazakov, M. Zgirski, E. Łusakowska, S. Kret, J. Korczak, T. Story, M. Sawicki, T. Dietl, *Phys. Rev. B* **100**, 041408(R) (2019).